COBEM UBERLÂNDIA 2019

ABCM Associação Brasileira de Engenharia e Ciências Mecânicas

25th ABCM International Congress of Mechanical Engineering
October 20-25, 2019, Uberlândia, MG, Brazil

COB-2019-1096
NON-LINEAR FINITE-ELEMENT BUCKLING ANALYSIS OF DRILL-STRINGS CONFINED IN VERTICAL WELLS

Lucas André dos Santos
Raphael Santana Silva
Thiago Gamboa Ritto
Universidade Federal do Rio de Janeiro (UFRJ); Av. Athos da Silveira Ramos, 274 - Cidade Universitária, Rio de Janeiro - RJ
lasantos@poli.ufrj.br; raphaelsantana@poli.ufrj.br; tritto@mecanica.coppe.ufrj.br

Abstract. *Drill-strings buckling has been for years an important concern on drilling engineering. Several analytical models have been developed and classical formulations are still used to predict this phenomenon on industrial applications. However, such equations often tend to oversimplify the real phenomenon and thus to produce results that may be distant from reality. This paper proposes a numerical analysis procedure to perform buckling analysis on drill-string columns confined in vertical wells. Linear and non-linear simulations are conducted using Abaqus Finite Element Analysis (FEA) software. The effect of drilling stabilizers, fluid and pipe to pipe contact is considered to permit a better approach to the real physical phenomenon. Comparison with analytical results and application to practical examples are made to demonstrate the accuracy of the proposed model. Finally, this article presents discussions on the impact of each model parameter considered.*

Keywords: *Buckling, Drilling, Finite Element Method, Post-buckling*

1. INTRODUCTION

Buckling analysis of drill-strings has been a subject of several investigations in the Oil & Gas field and arouses an even greater concern as wells exploration becomes more complex, for instance, in the Brazilian Pre-Salt formations. Huang *et al.* (2016) present among the possible consequences associated with such phenomenon: well deviation, casing wear, and drill string locking or failure. All these factors are ultimately associated with financial losses of different proportions.

Regarding classical buckling models, such as Euler's, drill-strings require a more complex analysis as they are influenced by additional parameters, such as gravity, immersion fluids, pipe-to-pipe contact interaction, well inclination, torque and drilling stabilizers. Analytical models developed in the last decades qualitatively agree on the evolution of buckling shapes as the *weight on bit* (WOB) is increased. After critical limits of compression, the column can collapse in different ways, initially assuming a lateral - sinusoidal - deformed shape and then, for greater values of WOB, a helical one.

Lubinski (1950) proposed the first buckling model applied to drill-strings in vertical wells. Subsequently, alternative analytical models presented new expressions for sinusoidal (Eq. (1)) and helical (Eq. (2)) critical buckling loads.

$$F_{sin} = \alpha (EI)^{1/3} w^{2/3} \tag{1}$$

$$F_{hel} = \beta (EI)^{1/3} w^{2/3} \tag{2}$$

where EI is the flexural rigidity of the column and w is the weight per unit length of the column. The multipliers α and β proposed by different authors are presented in Tab. 1. It is important to note that these multipliers are written in US units, commonly used in drilling operations.

Table 1. Values for α and β proposed by different authors for expressions of sinusoidal and helical critical buckling load in vertical wells.

Variable	Lubinski (1950)	Wang (1986)	Wu (1992)
α	1.94	1.018793	2.55
β	-	-	5.55

Experimental works already conducted in this area [Salies *et al.* (1993); Cunha *et al.* (1994)] have shown indeed the evolution of buckling modes through sinusoidal and helical shapes. However, the difficulty in holistically representing

such a complex phenomenon may generate analytical results that are distant from reality. More recent models using the Finite Element Method (FEM) [Hill and Datye (2011); Hajianmaleki and Daily (2014)] have shown better correlation with experimental results.

To analyze drill-strings with stabilizers, immersed in a drilling fluid, and subjected to normal and tangential contact interaction with an external casing, a new buckling analysis procedure using the FEM is proposed in this article. Initially, in *Case Study 1*, comparison with results available in the literature is made to validate the proposed model. Then, in *Case Study 2*, the analysis is extended to a 2500-m model representative of Brazilian's Pre-Salt formations.

2. METHODOLOGY

2.1 Computational methods

This study is conducted through numerical simulations using the FEM, a widely used method in the industry and academia to analyze the structural and mechanical behavior of systems. The commercial software ABAQUS 2018 is used as solver of the discretized equations representative of the buckling phenomenon.

ABAQUS disposes of two different, but usually complementary, ways to perform buckling simulations. Linear analysis - or *eigenvalue buckling analysis* - is appropriate to provide the critical buckling loads and, qualitatively, the mode shapes of rigid structures - subjected to little axial deformation prior to buckling. Non-linear analysis, usually succeeding the linear one, provide complete information on the collapsed structure and post-buckling.

Linear buckling analysis' core principle consists in identifying the singularities of the tangent stiffness matrix ($[K_t]$) representative of the discretized profile through a linear perturbation (Dassault Systèmes Team (2011)). Its solution provides the eigenvalues λ_i - critical loads - and the eigenvectors $\{\Phi_i\}$ - shapes - of each buckling mode.

$$([K_e] - \lambda[K_g])\{\Phi_i\} = 0 \tag{3}$$

where $[K_t]$ is composed by the elastic stiffness matrix $[K_e]$ and the geometric stiffness matrix $[K_g]$.

The analysis of structures containing geometrical, physical or boundary non-linearities, however, requires a different approach. Either Newton-Raphson or the Arc Length methods, both implemented in ABAQUS may be used to solve nonlinear equations; the first, with incremental loading or displacement procedure, and the second with Riks algorithm. In this study, displacement controlled Newton-Raphson analysis showed more suitability for post-buckling analysis.

In a post-buckling problem, the introduction of a geometric imperfection in the initial model is required to trigger a bifurcation in the structure's load-displacement behavior. Some options to modify the initially perfect geometry are introducing in the model (i) the geometrically imperfect shape of the real structure, if available, (ii) a linear combination of n buckling mode shapes previously obtained in linear analysis, or even (iii) a combination of dead loads. Obtaining realistic results strongly depends on a good estimate of imperfections.

Another relevant aspect in non-linear simulations is the application of numerical stabilization. ABAQUS provides an automatic mechanism for stabilizing unstable quasi-static problems through the automatic addition of volume-proportional damping to the model (Dassault Systèmes Team (2011)). As the added artificial damping affects the properties of the system's stiffness matrix, its effect on calculation results has to be controlled. Following Zhang *et al.* (2019), during the calculation process, a limit of 0.5 % was set for the proportion between numerical damping dissipation energy (ALLSD) and total strain energy (ALLIE) of the system.

2.2 Analysis Procedure

The base model used to conduct the two case studies presented in this article considers the physical problem of inserting a drill-string of initial length L_0 in a vertical well of same dimension, where a casing limits the radial displacement of the column. A summary of the characteristic boundary conditions of the problem is illustrated in Fig. 1 a); the evolution of the column compression problem - representatively hoisted by a hook - along the three different simulation steps is illustrated in Fig. 1 b). Length variation along each model is not represented in this simplified scheme.

This specific buckling problem can be understood as a trasition from a state of traction to a state of gradual compression as WOB is increased. This gradual compression is evidenced by the elevation of the transition point between traction and compression regions (H_n), remembering that the buckling phenomenon is precisely associated with the region of the column under compression. Drawing a parallel between the simulation steps and the actual physical situation, it can be understood that the end of the first step would correspond to the situation in which the drill-string has already reached the bottom of the well, but has its self weight completely supported by the hook load (WOB = 0). In the next two steps, the hook load is gradually reduced, which increases the WOB. After exceeding a certain critical value, WOB causes column buckling.

Describing in more detail each step of the simulation, in a first step, gravity - represented by the distributed load q - is applied to the model. Thus, the column takes on a new length of $L_1 = L_0 + \Delta L$ due to the tensile stress caused by its weight (W). In this step, exclusively, axial movement is allowed at the drill-string bottom node and fixed at the top node.

In deep wells, such as those present in the Brazilian Pre-Salt region, this freedom of movement is relevant because ΔL can reach values greater than 5 meters. Therefore, the starting point of the buckling study is a column under traction with a length of $L_1 > L_0$. Exemplifying with numerical values, a column with initial length L_0 = 2500m when fully supported by the hook load has an approximate effective length L_1 = 2502m.

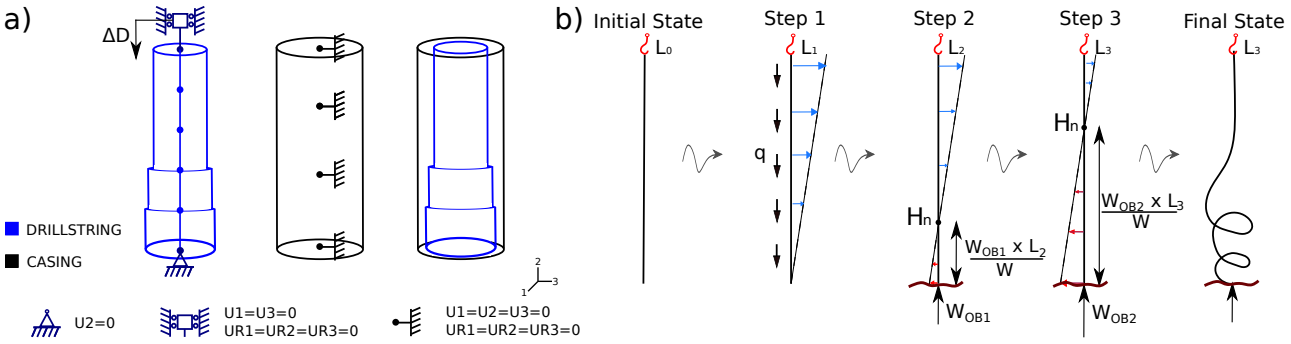

Figure 1. a) Illustrative scheme of the base model boundary conditions. b) Evolution of the column compression state along the analysis steps.

Then, in a second step, with boundary conditions presented in Fig. 1 a), a controlled displacement ΔD_1 is prescribed to the column upper node. From this prescribed displacement appears a compressive force (WOB > 0). In this way, the drill-string takes on a new length $L_2 = L_0 + \Delta L - \Delta D_1$. Ideally, ΔD_1 should be the maximum displacement that can be prescribed before the simulation encounters convergence problems and terminates prematurely. Exemplifying again with numerical values, after the first displacement prescription a column with L_1 = 2502m takes on a new length L_2 = 2501.7m; so, ΔD_1 = 0.3m. Assuming this is the prescribed displacement to initiate contact interaction between the tubes, if ΔD_1 far superior than 0.3m were chosen, the simulation would end due to convergence problems. This would prevent analyzing, for example, drill-string behavior for a prescribed displacement of 1.0m. This is the reason for fractioning the displacement prescription into two or more steps, using a numerical stabilization to allow the simulation to continue.

In a third step, a controlled displacement ΔD_2 is prescribed to the column upper node. In this way, it takes on a new length $L_3 = L_0 + \Delta L - \Delta D_1 - \Delta D_2$. This prescribed displacement results in an even larger increase of the WOB and is applied after buckling, when the drill-string initiates contact interaction with the casing. Thus, this third step aims to allow the continuation of the second step through the use of a certain degree of numerical stabilization. As discussed in Sec. 2.1, artificial damping can ease the solution of non-linear problems without changing its results as long as the dissipated energy is guaranteed to be small compared to the total internal energy of the system. In this work, this step is fundamental so that it is possible to observe the formation of helical buckling modes. Taking the same example as above, after the second displacement prescription a column with L_2 = 2501.7m takes on a new length L_3 = 2501.0m; so, ΔD_2 = 0.7m and $\Delta D_1 + \Delta D_2$ = 1.0m. If it were necessary to prescribe an even greater displacement, one possibility would be to create a fourth step using a higher degree of stabilization.

3. CASE STUDY 1: VERIFICATION MODEL

This section presents the buckling analysis of a small-scale drill-string model studied experimentally by Cunha *et al.* (1994) and replicated later by Hill and Datye (2011) and Hajianmaleki and Daily (2014). The objective is to compare the results generated by the FEM model developed in this article with results available in the literature in order to verify its validity.

3.1 Geometry and Model

A steel pipe ASTM T-304-W-B, with 16.33 meters (643") in length, 6.35 millimeters (0.25") of outside diameter (OD) and 5.33 mm (0.21") of inside diameter (ID) simulated the drill-string while a Plexiglas tube with 16.33-m (643") in length and 76.2 mm (3") of ID was chosen to simulate the casing. As the external tube OD was not provided by Cunha *et al.* (1994), an 86.2 mm (3.4") OD was assumed to minimize casing deformation and, consequently, side effects generated on the internal tubing buckling. Both tubes are oriented vertically and subjected to the boundary conditions presented in Sec.2.2. Each geometry is modeled using 100 three-dimensional linear Timoshenko beam (B31) elements. A convergence study was performed on the number of elements and the results showed a difference less than 1% to the models of finer mesh. The steel tubing material is modeled using an elastic constitutive relationship with a Young's modulus of 206.8 GPa and a Poisson's ratio of 0.3 with a density of 7810 kg/m^3. For this analysis, stresses remain below the steel elastic limit.

The interaction between internal and external pipes is modeled using three-dimensional tube-to-tube contact (ITT31)

elements - assigned to the internal pipe - and slide line contact (SLIDELINE) elements - assigned to the confining hole. The normal contact between tubes is modeled using *Hard Contact* formulation and the tangential interaction considers *Coulomb Friction* formulation with a coefficient of 0.38 - as supplied in Cunha *et al.* (1994). For comparison purposes, the friction coefficient is varied to observe the influence of this parameter on the obtained results.

Geometric imperfections are introduced as the linear combination of two distributed "dead loads", with sinusoidal shape, applied in two orthogonal vertical planes (Fig. 2), what creates three-dimensional imperfections. As pointed by Hill and Datye (2011), this is a necessary condition to observe a further transition to helical buckling modes. At the same time, it is reasonable to consider that a real structure would have geometrical imperfections in more than one single plane. This procedure for introducing imperfections is performed in an extra step of the simulation - not presented in Sec. 2.2 - between the first and second steps.

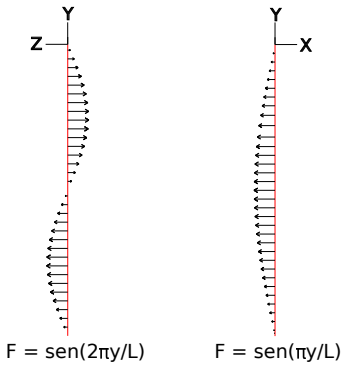

Figure 2. Ilustration of "dead loads" defined in XY and YZ planes.

3.2 Results and Discussion

To obtain convergence in the results, special attention is given to the choice of prescribed displacement values. Using the variables defined in Sec. 2.2 , $L_0 = 16.33m$, $\Delta L = 0.049mm$, $\Delta D_1 = 0.3mm$ and $\Delta D_2 = 9mm$. The time increment control should also be properly controlled to minimize numeric problems associated with pipe-to-pipe contact.

In Fig. 3, both graphs represent the drill-string Load x Displacement behavior, with load measured in the axial direction at the drill-string bottom node - therefore, corresponding to WOB - and displacement measured in the axial direction at the drill-string top node. The number of elements was determined from the mesh convergence study presented in Fig. 3 a), where similar behavior is observed for models above 50 elements. In Fig. 3 b) the influence of friction on the results is observed and, in Fig. 4, the deformed shape for Fig. 3 b) loads at points A-H is presented.

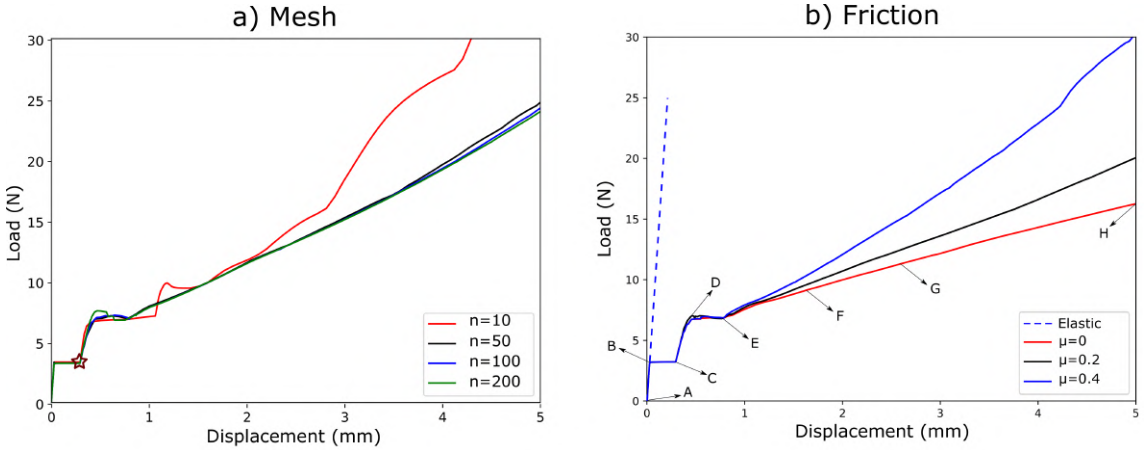

Figure 3. a) Axial Load (N) *vs.* Axial Displacement (mm) for models with different mesh refinement; b) Axial Load (N) *vs.* Axial Displacement (mm) for three different coefficients of friction and transition points for the situation without friction. *Elastic* function is the linear reference with inclination (EA/L).

For each point, the following aspects can be noted: at Point A, in the absence of WOB, the column is in its initial state, in which the only existing deformations are due to initial imperfections and gravity. At point B, WOB reaches a first critical value and sinusoidal buckling occurs. At this point, the flexural stiffness of the column approaches zero and allows radial displacement of the column with practically constant WOB, until the contact interaction with the casing starts (Point C). At point C, the stiffness of the column turns to increase and, with an increment of WOB, at point D its deformed shape

takes on a three-dimensional aspect that evolves with rigidity close to zero up to point E. At this point, it can be seen in Fig. 5 b) the beginning of a region of approximately linear behavior that evolves to the point H. Until then, the influence of friction was practically negligible. However, the development of a helical buckling mode - characterized by increasing contact between column and casing - causes a more pronounced growth of stiffness for situations with greater friction.

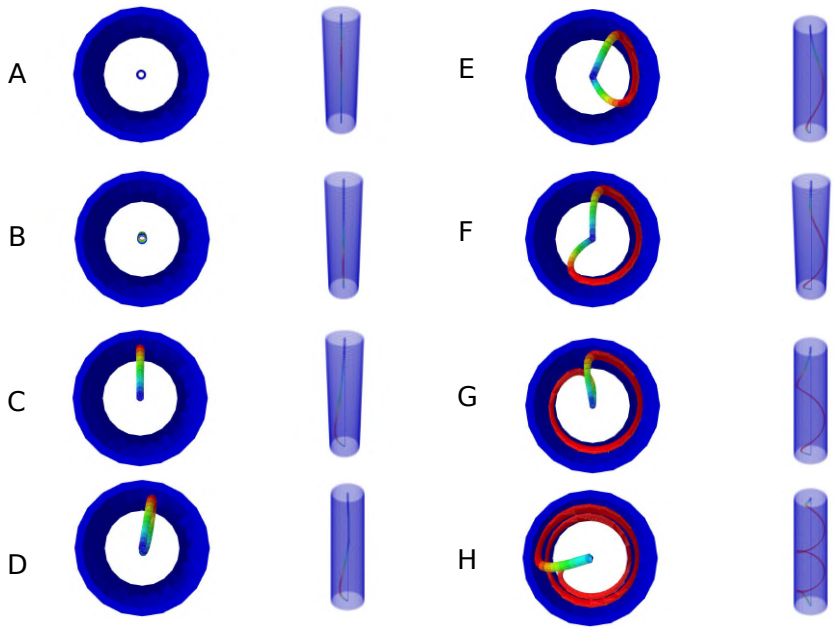

Figure 4. Bottom and isometric views of buckling shapes A-H presented in Fig. 3 b).

In Fig. 5 a), the influence of initial geometric imperfections magnitude on the results for a coefficient of friction μ = 0.38 is presented. Amplifying the region highlighted in Fig. 5 a), Fig. 5 b) is obtained. The imperfections value represents the maximum distance measured in meters from the neutral axis of the pipe. The star represents the points of contact initiation between the inner and outer tubes in each model, caused by the buckling of the inner tube. From this graph, the critical sinusoidal buckling load (F_{sin}) is identified as the load at which the stiffness of the column becomes zero.

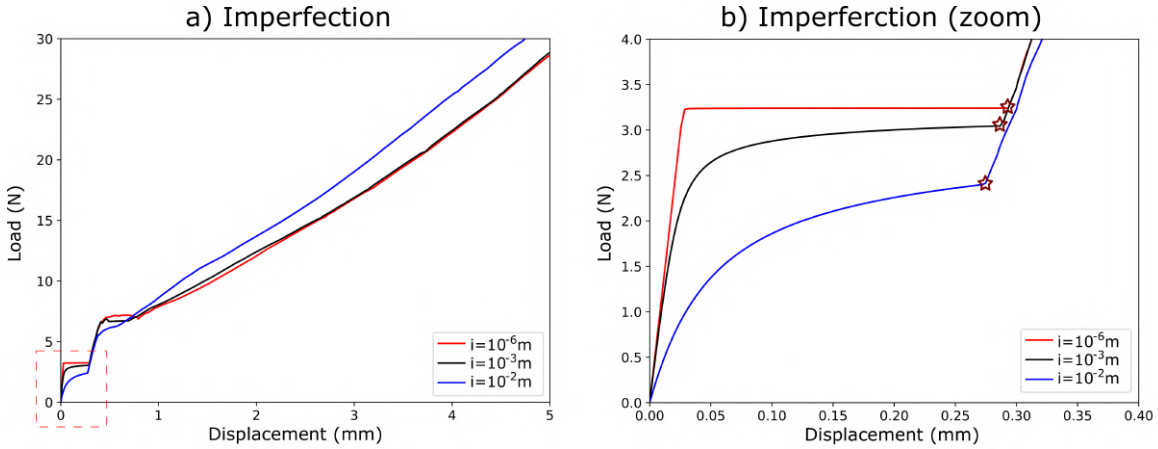

Figure 5. a) Axial Load (N) *vs.* Axial Displacement (mm) for models with different imperfection magnitudes; b) Amplification of region outlined in a).

It is observed that as the imperfections in a given model decrease, the transition between pre-buckling - elastic stiffness - and post-buckling - zero stiffness - states becomes more abrupt. For the model with 10^{-6} m imperfections, it is easy to determine F_{sin} as approximately 3.2N. On the other hand, the determination of a specific load becomes more complicated when analyzing the other models, since there is a gradual loss of stiffness according to the prescribed displacement. A null rigidity point may not even exist; at the same time, it cannot be stated that there is no buckling for these situations. It only becomes necessary to update the buckling definition for such cases. In Case Study 1, F_{sin} is defined as the load at which contact initiates - point C - and F_{hel} as the load for which a complete helix pitch is fully developped at the drill-string - point G. Such considerations are consistent with the experimental work of Cunha *et al.* (1994), used as a reference for

comparison of results.

Before presenting the values obtained for F_{sin} and F_{hel} in this work, Tab. 2 compares the experimental results of Cunha *et al.* (1994) to analytical, experimental and numerical values available in the literature for analysis of the same geometry. It is important to note that the analytical models presented here disregard geometric imperfections and friction; the experimental models include geometric imperfections and a coefficient of friction $\mu = 0.38$; and the numerical models seek to follow, as much as possible, the experimental ones. For sinusoidal loads, the analytical results obtained are higher than the experimental ones, which is consistent with the observations made in Fig. 5 a), since geometric imperfections are null in analytical models. The numerical results have a good correlation with the experimental ones, being the existing differences attributed to the modeling of geometric imperfections. For helical loads, analytical and numerical results are more distant from experimental ones, which can be explained by the greater nonlinearity until the formation of a helix pitch in the column.

Table 2. Comparison between experimental results obtained by Cunha *et al.* (1994) and analytical, numerical and experimental results available in the literature.

Sinusoidal

Analytical	F_{sen} (N)	Error (%)
Lubinski (1950)	3.14	29.7
Wang (1986)	1.79	26.0
Wu (1992)	4.12	70.2
Experimental		
Cunha *et al.* (1994)	2.42	Ref.
Hill and Datye (2011)	1.69	-
Numerical (FEA)		
Hill and Datye (2011)	2.14	11.6
Hajianmaleki and Daily (2014)	2.93	21.1

Helical

Analytical	F_{hel} (N)	Error (%)
Wu (1992)	8.97	24.9
Experimental		
Cunha *et al.* (1994)	11.94	Ref.
Numerical (FEA)		
Hajianmaleki and Daily (2014)	8.49	28.9

Then, in Tab. 3 the values obtained in this work are presented. A data organization similar to the one presented in Tab. 2 is adopted, however presenting the results as a function of two variables: coefficient of friction (μ) and geometric imperfections magnitude (i). This additional consideration is made because, as noted in Fig. 3 b) and Fig. 5 a), while F_{sin} only depends on geometric imperfections, F_{hel} depends on both the friction coefficient and imperfections.

Table 3. Comparison between experimental results obtained by Cunha *et al.* (1994) and results obtained in this work.

Sinusoidal

		$i = 10^{-6}$ m		$i = 10^{-3}$ m		$i = 10^{-2}$ m	
Numerical (FEA)	μ	F_{sin} (N)	Error (%)	F_{sin} (N)	Error (%)	F_{sin} (N)	Error (%)
This work	0.38	3.21	32.6	3.04	25.6	2.41	0.4

Helical

		$i = 10^{-6}$ m		$i = 10^{-3}$ m		$i = 10^{-2}$ m	
Numerical (FEA)	μ	F_{hel} (N)	Error (%)	F_{hel} (N)	Error (%)	F_{hel} (N)	Error (%)
This work	0.38	15.27	27.9	15.53	30.1	17.75	48.6
This work	0.20	12.90	8.0	13.00	8.9	14.22	19.1

For sinusoidal loads a smaller error is obtained for the model with imperfections of 10^{-2} m, which is a physically conceivable value for a 16.33 meter long column. For helical loads, with μ = 0.38 results distant from the experimental value are obtained. Since there is no description about the method applied to obtain this coefficient of friction in Cunha *et al.* (1994), its validity can be questioned. Thus, for comparison purposes, a new analysis with a slightly lower coefficient of friction is performed and values closer to the experimental ones are obtained.

Finally, the model presented in this article provided results consistent with the adopted reference - Cunha *et al.* (1994). However, a deeper comparison, further investigating experimental friction coefficient and geometrical imperfections, would be desirable in order to validate this work's model and increase its reliability.

4. CASE STUDY 2: REAL-WORLD DRILL-STRING MODEL

This section presents the buckling analysis of a real-scale column model representative of deep wells in the Brazilian Pre-Salt region. The objective is to apply the procedure developped in this article to a real drill-string geometry and compare the results generated with models available in the literature, unable to analyze more complex situations considering friction, cross section changes and motion stabilizers.

4.1 Geometry and Model

The drill string under analysis has 2500 meters in length, variable cross section and is confined into a casing with a uniform internal diameter of 21.25". Both tubes are subjected to the boundary conditions presented in Fig. 1. A complete overview of the studied geometry is presented in Tab. 4.

Table 4. Real-world based drillstring model dimensions.

Part	OD (in)	ID (in)	Length (m)
Drillpipe	5.875	5.045	2180.77
HWDP	5.875	4	111.11
Drillcollar 3	8	3	115.55
Drillcollar 2	9.5	2.875	61.28
Stabilizer 2	17.375	3.125	2.35
Drillcollar 1	10	4	7.52
Stabilizer 1	17.375	6.25	0.99
MWD	10	3	20
Drillbit	17.5	3.5	0.43
Total			**2500**

Each geometry is modeled using 1300 three-dimensional linear beam (B31) elements non-uniformly distributed along the column. A convergence study was performed on the number of elements and the results showed a difference less than 1% to the models of finer mesh. The steel tubing material is modeled using an elastic constitutive relationship with a Young's modulus of 206.8 GPa and a Poisson's ratio of 0.3 with a density of 7850 kg/m^3. For this analysis, stresses remain below steel elastic limit. The interaction between internal and external pipes follows the same guidelines defined Sec. 3.1, with a friction coefficient of 0.3. The buoyancy effect generated by the 11 lbm/gal specific mass drilling mud is modeled by changing the tubing equivalent specific mass to 6532 kg/m^3 - following Eq. 2 presented in Mitchell (1988). The definition of geometric imperfections follows the same procedure as Sec. 3.1; a "dead load" with maximum amplitude 10^{-3}N defined as Fig. 2 results in a structure with imperfections of the order 10^{-4}m, which was sufficient to trigger the column buckling.

4.2 Results and Discussion

To obtain convergence in the results, it remains valid the same observations made in the Sec. 3.2 about (i) choosing prescribed displacement values, (ii) controlling maximum time increment, and (iii) adding numerical stabilization. The first result, presented in Fig. 6 a), shows how to identify the crictical buckling load in this new geometry. Initially, a difference can be already noted between the model studied in this section and *Case Study 1*: both curves, related to models with different casing internal diameters (ID), seem to be approximately linear within the studied range, which differs from the curves presented in Fig. 3, in which there are visible regions with approximately zero stiffness relative to the evolution of different buckling modes. However, it is important to remember that the scale of the graphs between the two case studies is different. In Fig. 6 b) - amplification of the region outlined in Fig. 6 a) - it is still possible to identify less stiffer regions around 320kN, what characterizes buckling.

A second result analyzed in this section is the influence of motion stabilizers positioning upon drill-string critical load. The critical load corresponds to the regions presented in Fig. 6 a) where there is a sudden drop in stiffness. In the deformed view, it corresponds approximately to the load where contact between Bottom Hole Assembly (BHA) and casing is initiated. It is worth noting that, although stabilizers are located in the BHA, their contact with the casing is expected and occurs before the crictical buckling load.

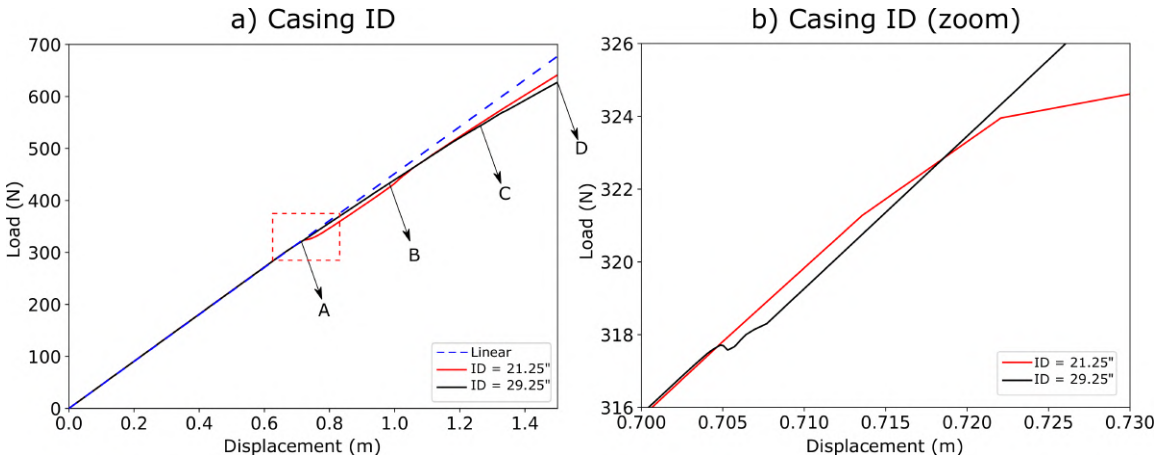

Figure 6. a) Axial Load (kN) vs. Axial displacement (m) for models with different casing ID; b) Amplification for region outlined in a).

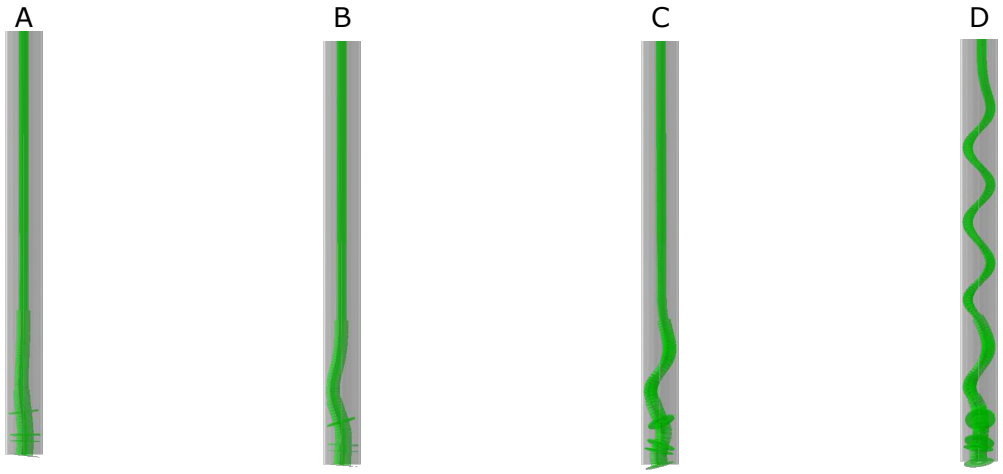

Figure 7. Deformed views for points A-D identified in Fig. 6.

Four column models are defined, each with a different positioning of stabilizers. The model *Initial* corresponds to the geometry defined in Tab. 4, where it is desired to reposition stabilizers in order to increase the WOB for contact. The model *W/o stabilizers* corresponds to *Initial*, but without stabilizers; stabilizers removal was accomplished by reducing *Stabilizer 1* and *Stabilizer 2* ODs to 10in, the same as *Drillcollar 1*.

Table 5. Results of stabilizers repositioning procedure.

Model	**Initial**	**W/o stabilizers**	**Positioning 1**	**Positioning 2**
Number of Stabilizers	2	0	1	2
Stabilizers position (m)	21; 30	-	62	30; 62
Load for contact - WOB_c (kN)	240	73	170	338
Contact position (m)	93	71	27	103
Part on contact	Drillcollar 2	Drillcollar 2	Stabilizer 2	Drillcollar 3

Running a first analysis with the model *W/o stabilizers*, the first point of contact between BHA and casing is identified. Then, model *Positioning 1* is created by positioning one stabilizer in this region in order to shift the contact for a higher WOB. It is worth to note that this positioning is not made in the exact location of the contact point because it must respect the original BHA tools length at this position. And by executing a similar procedure with model *Positioning 1*, model *Positioning 2* is created with a second stabilizer position defined. Tab. 5 presents the results for each model and Fig. 8 shows the deformed shape of each model in its critical situation with a magnification of 100x showing the region between *Drillcollar 3* and *Drillbit*. The deformed shapes presented here, in Fig. 6 would correspond approximately to the regions on the curves characterized by a sudden drop in stiffness. It is worth to emphasize that, despite the aspect of a disk, the dimensions applied to stabilizers and drillbit remain those specified in Tab. 4.

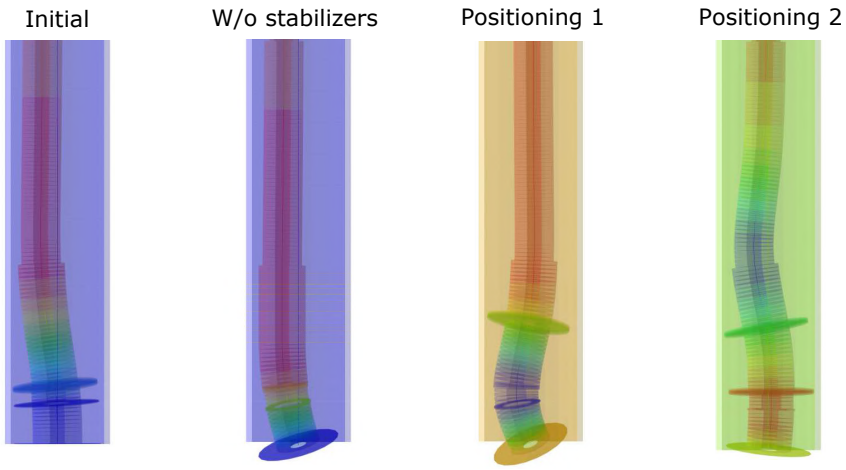

Figure 8. Front view of the contact between BHA and Casing for each model studied when the crictical buckling load is attained.

In *Case Study 2*, simulations varying friction and drilling fluid density were also conducted. However, differently from *Case Study 1* their influence is barely visible on a Load *vs.* Displacement graph, resulting in minor sudden stiffness variations. These parameters would be more important for drill-string lock-up analysis, but it goes beyond the objectives of this work.

5. CONCLUSIONS

In this paper, an analysis procedure for buckling analysis using the finite element method is discussed. Some important remarks extracted from the results are:

- Friction affects only helical buckling loads, while geometrical imperfections affect both sinusoidal and helical crictical buckling loads;
- Good correlation with experimental results may be obtained with good estimates of model's friction coefficient and geometric imperfections;
- Buckling does not imply necessarily a null stiffness region on a Load vs. Displacement curve, but rather a sudden drop in stiffness;
- Motion stabilizers positioning may increase a drill-string crictical buckling load;

6. REFERENCES

Cunha, J., Salies, J., Petrobrás, U. of Tulsa, Azar, J. and Soren Jr, J., 1994. "Experimental and Analytical Study of Sinusoidal Buckling in Vertical Wells". *SPE*, , No. 2, pp. 77–85.

Dassault Systèmes Team, 2011. *Abaqus/ CAE User's Manual*. Dassault Systèmes, Providence, USA. URL `https://www.simulia.com/`.

Hajianmaleki, M. and Daily, J.S., 2014. "Critical-Buckling-Load Assessment of Drillstrings in Different Wellbores by Use of the Explicit Finite-Element Method". , No. September 2013, pp. 3–6.

Hill, L.T. and Datye, D.V., 2011. "First-principles finite element modelling of coiled tubing in directional wells". *ASME International Conference on Ocean, Offshore and Arctic Engineering*, pp. 1–5.

Huang, W., Gao, D. and Liu, Y., 2016. "A study of tubular string buckling in vertical wells". *International Journal of Mechanical Sciences*, Vol. 118, No. September, pp. 231–253. ISSN 0020-7403. doi:10.1016/j.ijmecsci.2016.09.035. URL `http://dx.doi.org/10.1016/j.ijmecsci.2016.09.035`.

Lubinski, A., 1950. "A Study of the Buckling of Rotary Drilling Strings". , No. March.

Mitchell, R.F., 1988. "New Concepts for Helical Buckling". , No. September, pp. 303–310.

Salies, J.B., Azar, J.J. and Sorem, J.R., 1993. "Experimental and Mathematical Modeling of Helical Buckling of Tubulars in Directional Wellbores". *SPE Annual Technical Conference and Exhibition*, , No. 386, pp. 433–443.

Wang, C.Y., 1986. "A critical review of the heavy elastica". *Pagamon Journals Ltd.*, Vol. 28, No. 8, pp. 549–559.

Wu, J., 1992. *Buckling behavior of pipes in directional and horizontal wells*. Phd dissertation, Texas AM University.

Zhang, Z., Liu, H. and Chen, Z., 2019. "Lateral Buckling Theory and Experimental Study on Pipe-in-Pipe Structure". *Metals 2019*. doi:10.3390/met9020185.